Chemical Science

Accepted Manuscript

This article can be cited before page numbers have been issued, to do this please use: R. E. MacKenzie, T. Hajdu, J. Seed, G. F. S. Whitehead, R. W. Adams, N. F. Chilton, D. Collison, E. J. L. McInnes and C. A. P. Goodwin, *Chem. Sci.*, 2024, DOI: 10.1039/D4SC03005B.

ROYAL SOCIETY OF CHEMISTRY

rsc.li/chemical-science

δ-Bonding Modulates the Electronic Structure of Formally Divalent nd^1 Rare Earth Arene Complexes

View Article Online
DOI: 10.1039/D4SC03005B

Ross E. MacKenzie,[1,2] Tomáš Hajdu,[2] John A. Seed,[1,2] George F. S. Whitehead,[2] Ralph W. Adams,[2] Nicholas F. Chilton,[2,3] David Collison,[2] Eric J. L. McInnes,[2] Conrad A. P. Goodwin*[1,2]

[1] Centre for Radiochemistry Research, The University of Manchester, Oxford Road, Manchester, M13 9PL (UK).

[2] Department of Chemistry, The University of Manchester, Oxford Road, Manchester, M13 9PL (UK).

[3] Research School of Chemistry, The Australian National University, Sullivans Creek Road, Canberra, 2601 (Australia).

*Correspondence: conrad.goodwin@manchester.ac.uk

View Article Online
DOI: 10.1039/D4SC03005B

Abstract

Landmark advances in rare earth (RE) chemistry have shown that divalent complexes can be isolated with non-Aufbau $4f^n\{5d/6s\}^1$ electron configurations, facilitating remarkable bonding motifs and magnetic properties. We report a series of divalent *bis*-tethered arene complexes, [RE(NHAr$^{i\text{Pr6}}$)$_2$] (**2RE**; RE = Sc, Y, La, Sm, Eu, Tm, Yb; NHAr$^{i\text{Pr6}}$ = {N(H)C$_6$H$_3$-2,6-(C$_6$H$_2$-2,4,6-*i*Pr$_3$)$_2$}). Fluid solution EPR spectroscopy gives $g_{iso} < 2.002$ for **2Sc**, **2Y**, and **2La**, consistent with formal nd^1 configurations, calculations reveal metal-arene δ-bonding *via* mixing of n$d_{(x2-y2)}$ valence electrons into arene π* orbitals. Experimental and calculated EPR and UV-Vis-NIR spectroscopic properties for **2Y** show that minor structural changes markedly alter the metal $d_{(x2-y2)}$ contribution to the SOMO. This contrasts $4f^n\{5d/6s\}^1$ complexes where the valence *d*-based electron resides in a non-bonding orbital. Complexes **2Sm**, **2Eu**, **2Tm**, and **2Yb** contain highly-localised $4f^{n+1}$ ions with no appreciable metal–arene bonding by density functional calculations. These results show that the physicochemical properties of divalent rare earth arene complexes with both formal nd^1 and $4f^{n+1}$ configurations are nuanced, may be controlled through ligand modification, and require a multi-pronged experimental and theoretical approach to fully rationalise.

DOI: 10.1039/D4SC03005B

Introduction

A hallmark of trivalent lanthanide ions is the relative insensitivity of valence 4*f*-orbitals to the coordination environment. While this gives rise to useful physical and optical properties, such as their narrow optical emission profiles and large magnetic moments from their unquenched orbital angular momentum, the weakness of this interaction also inhibits the extent to which their properties may be tailored through molecular design. Advancements in divalent molecular rare earth and lanthanide (Sc, Y, La–Lu; collectively Ln henceforth) chemistry have shown that in coordination environments such as $[Ln(Cp^R)_3]^-$ or $[Ln(Cp^R)_2]$ (Cp^R = substituted cyclopentadienide ligands), Ln(II) complexes can be isolated with $4f^n5d^1$ or $4f^n\{5d/6s\}^1$ valence electron configurations, at least for La–Lu, while Sc and Y necessarily give $3d^1$ or $4d^1$ ions.[1-23] Further work shows these non-Aufbau ions can be exploited as potential qubit candidates,[15-17] exhibit record-setting magnetic properties,[18-20] and have produced the first examples of molecular Ln–Ln bonding outside of endohedral fullerenes.[20-22] Similar advancements have also been made with actinide elements.[24] However, with few exceptions, design strategies employed to isolate examples of these ions use geometries (*e.g.* C_{3h} or D_{5h}) that minimise or forbid, by symmetry, the mixing of 5*d* (or 5*d*/6*s* hybridised) valence electrons with ligand orbitals. This is useful in some applications,[15-17] but in analogy to the poor tunability of 4*f*-orbitals in Ln(III) ions, it limits the extent to which the electronic structures of $4f^n5d^1$ or $4f^n\{5d/6s\}^1$ Ln(II) complexes may be controlled through ligand design.

Using ligand field principles commonplace in the *d*-block that also apply to $4f^n5d^1$ Ln(II) ions, we may instead target molecular designs where the electronic structure and physicochemical properties are more sensitive to changes in the coordination environment. Arene ligands provide a promising route towards these goals due to their ability to act as symmetry-allowed donors into vacant *d*-orbitals, and further stabilise lower oxidation states

View Article Online
DOI: 10.1039/D4SC03005B

through back donation.[25-30] Indeed, the only examples of formally zero-valent rare earth complexes are within $[M(\eta^6\text{-}C_6R_6)_2]$ frameworks.[31-35]

Herein, we present a series of structurally analogous *bis*-tethered arene divalent rare-earth complexes of the form $[M(NHAr^{iPr6})_2]$ (**2M**, M = Sc, Y, La, Sm, Eu, Tm, Yb; $NHAr^{iPr6}$ = $\{N(H)C_6H_3\text{-}2,6\text{-}(C_6H_2\text{-}2,4,6\text{-}i\text{Pr}_3)_2\}$) – the synthesis and some properties of **2Y** have been reported previously.[36] In all cases, characterisation using SQUID magnetometry, solid and solution phase EPR spectroscopy, UV-Vis-NIR spectroscopy, density functional theory (DFT) and complete active space self-consistent field (CASSCF) calculations support the description of these as formal Ln(II) complexes, demonstrating that this framework is robust across a range of Ln(II) ion sizes and (formal) reduction potentials. While all seven divalent complexes display close metal–arene contacts, only **2Sc**, **2Y**, and **2La** show mixing of a metal valence $nd_{(x2\text{-}y2)}$ orbital with the arene π* to give δ-bonding interactions. Complexes **2Sm**, **2Eu**, **2Tm**, and **2Yb** instead adopt metal-localized $4f^{n+1}$ configurations in accordance with their large Ln(II) $4f^{n+1} \rightarrow 4f^n5d^1$ promotional energies.[37, 38] Solid and solution phase UV-Vis-NIR and EPR for **2Y**, combined with DFT calculations, reveals that the balance of metal *vs* arene-centred spin-density is sensitive to small structural changes between these phases, suggesting the properties of divalent rare earth complexes with nd^1 may be tuned through ligand design.

View Article Online
DOI: 10.1039/D4SC03005B

Results and Discussion

Synthesis

A reductive route was pursued for the synthesis of **2M** (M = Sc, Y, La, and Tm; **Scheme 1A**), which began with the synthesis of trivalent [M(NHAr^{iPr6})$_2$(I)] (**1M**, M = Sc, Y, La, Tm) precursors. Complexes **1M** were synthesized by salt elimination between KNHAr^{iPr6} (refs. [39, 40]) and the relevant rare earth tri-iodide salt MI$_3$(THF)$_n$ (*n* = 4, M = La; *n* = 3.5, M = Y, Tm; *n* = 3, M = Sc) in Et$_2$O.[41] Workup and crystallisation from toluene gave fair to good crystalline yields (47–62%). ^{1}H NMR spectroscopy of diamagnetic **1Sc**, **1Y**, and **1La** in d_6-benzene show the M···C$_{6\text{-arene}}$ interaction is dynamic in solution and that all four Tripp groups are in exchange (see *Supporting Information* for detailed assignments).[36]

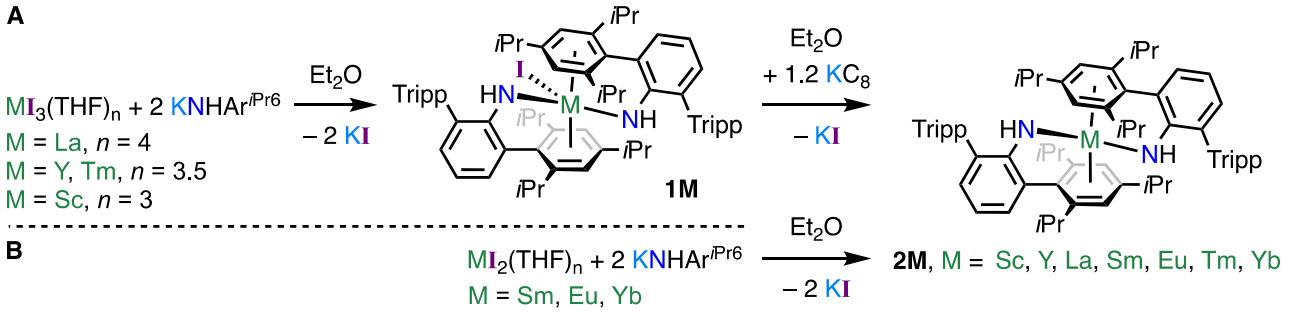

Scheme 1. Synthesis of (Route **A**) [M(NHAr^{iPr6})$_2$(I)] (**1M**, M = Sc, Y, La, Tm), and (Route **B**) [M(NHAr^{iPr6})$_2$] (M = Sc, Y, La, Sm, Eu, Tm, Yb). Tripp = {C$_6$H$_2$-2,4,6-*i*Pr$_3$}.

Reduction (KC$_8$, 1.2 equiv.) of **1M** (M = Sc, Y, La, Tm) in Et$_2$O gave, after workup and crystallization from Et$_2$O, dark crystals of **2M** in poor to fair yields (shown as % yield ahead): **2Sc** (red, 53%), **2Y** (red/green, 55%), **2La** (red/brown, 45%), and **2Tm** (red/brown, 65%). Salt elimination between KNHAr^{iPr6} and MI$_2$(THF)$_2$ (M = Sm, Eu, Yb)[42] in Et$_2$O gave poor to excellent isolated crystalline yields of **2Sm** (69%), **2Eu** (20%), and **2Yb** (82%) (**Scheme 1B**). Attempts to synthesise **1Sm** and **1Yb** using MI$_3$(THF)$_n$ precursors were unsuccessful,

leading to intractable mixtures (see *Supporting Information*), and we did not attempt the synthesis of **1Eu**.

View Article Online
DOI: 10.1039/D4SC03005B

While the ^{1}H NMR spectra of **1Sc**, **1Y**, and **1La** showed the metal-bound and "terminal" {C_6H_2-2,4,6-*i*Pr$_3$} (Tripp) groups were in exchange at room temperature, the spectrum of diamagnetic **2Yb** in d_6-benzene shows six doublets for the CH_3-*i*Pr groups, along with a single N(H) resonance. Thus, **2Yb** is C_2 symmetric in solution and the Tripp groups do not appreciably exchange at room temperature. This does not appear to be due to steric hinderance as the Sc(III) in **1Sc** is smaller than Yb(II) (6-coordinate radii: Yb(II), 0.868 Å; Sc(III), 0.745 Å). A variable temperature ^{1}H NMR study in d_8-toluene shows the CH_3-*i*Pr peaks begin to coalesce at 308 K, but full equilibrium is not reached until *ca*. 358 K (**Figures S40** and **S41**). The ^{171}Yb–^{1}H HMBC NMR spectrum gave two cross-peaks at δ_{171Yb} = –83 ppm (δ_{1H} = 3.53 and 7.02 ppm), showing the ^{171}Yb couples to both the anilido proton and the Tripp 3,5-CH groups. The ^{1}H NMR spectra of paramagnetic **2M** complexes were uninformative, see the *Supporting Information* for all NMR spectra.

Molecular structures

Single crystal X-ray diffraction studies on **1M** (M = Sc, Y, La, Tm) show all crystallize in the triclinic space group $P\bar{1}$ (Z' = 1) and are *pseudo* three-coordinate – see **Figure 1**. In **1La**, the metal is sandwiched almost equally between two Tripp groups (La···$C_{6\text{-centroid}}$ = 2.8714(12) and 2.8783(12) Å; La···N_2I plane deviation = 0.0042(15) Å). Conversely, **1Sc** and **1Y** have a single Tripp group close to the metal (M···$C_{6\text{-centroid}}$: **1Sc**, 2.3391(8) Å; and **1Y**, 2.4949(9) Å) and hence are trigonal pyramidal. The structure of **1Y** is comparable to recently reported [Y(NHAr$^{i\text{Pr6}}$)$_2$(Cl)].[36] See the *Supporting Information* for the structure of **1Tm**, and a comparison of **1M** complexes. In the following sections, we shall continue to use

the term "$C_{6\text{-centroid}}$", noting it is not strictly appropriate to define a centroid for non-planar groups.

View Article Online
DOI: 10.1039/D4SC03005B

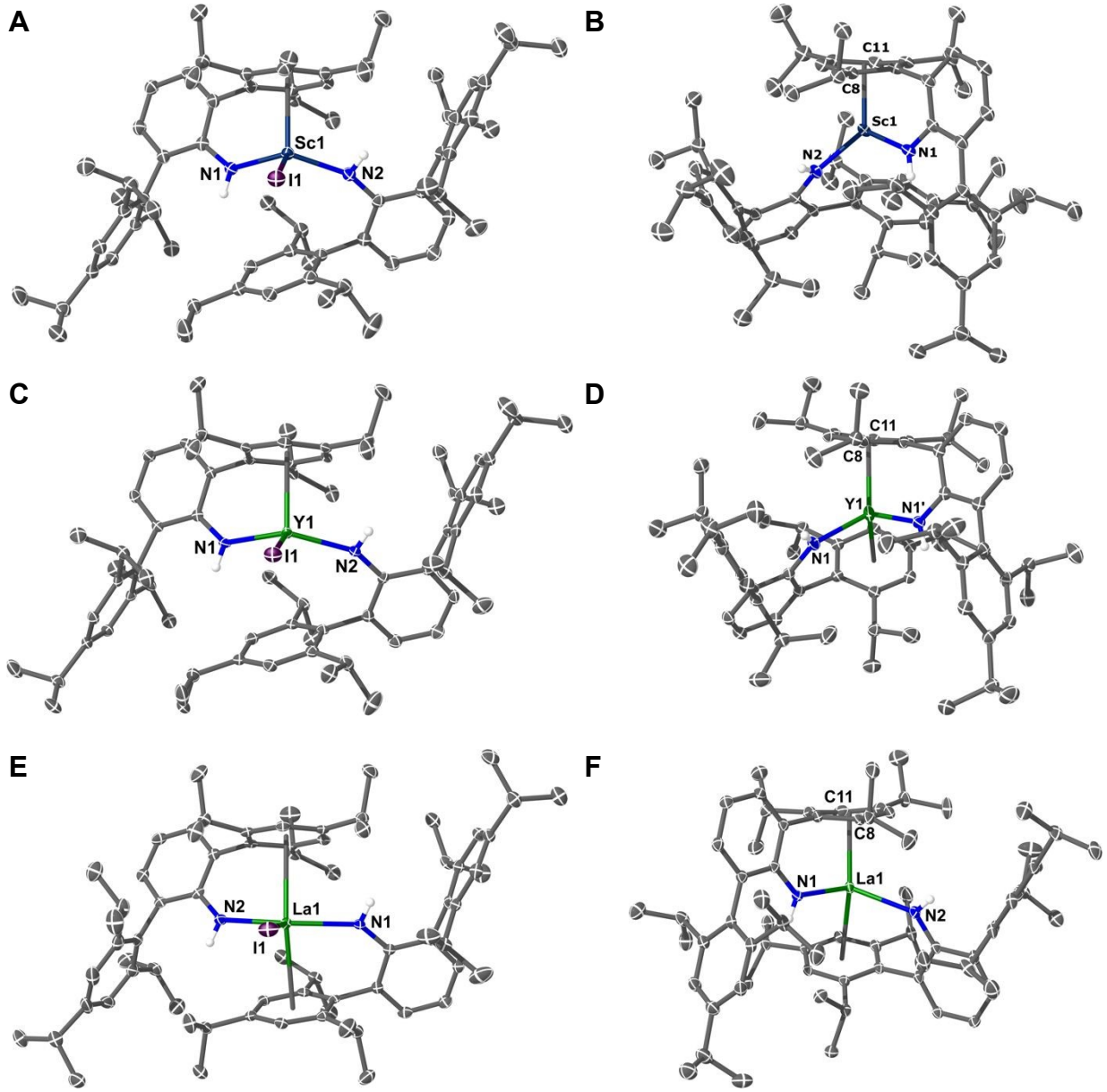

Figure 1. Molecular structures: (A) **1Sc**; (B) **2Sc**; (C) **1Y**; (D) **2Y**; (E) **1La**; (F) **2La**. Thermal ellipsoids have been set at 40% probability. H-atoms except those on N–H groups, solvents of crystallization, and disordered components have been removed for clarity.

The molecular structures of **2Sc**, **2Y**, and **2La** are also shown in **Figure 1** (see *Supporting Information* for **2Sm**, **2Eu**, **2Tm**, and **2Yb**). With the exception of **2Sc**, all **2M** complexes (M

View Article Online
DOI: 10.1039/D4SC03005B

= Y, La, Sm, Eu, Tm, Yb) show two Tripp groups closely approaching the metal. When viewed along the $C_{6\text{-centroid}}\cdots C_{6\text{-centroid}}$ axis these groups are either fully eclipsed due to crystallographic C_2 symmetry (**2Y**, **2Eu**, and **2Yb**), or are *pseudo*-eclipsed (**2Sc**, **2La**, **2Sm**, and **2Tm**). In **2Sc**, only one Tripp group is close to the metal. The nature of this metal-arene interaction provides insight into the electronic structure *vis-à-vis* metal- or ligand-centred reduction.[43, 44] Complexes **2Sc** and **2La** crystallize with a whole molecule in the asymmetric unit, and in both one metal-bound Tripp group is non-planar, showing an "open book" deformation for which a "hinge angle" ($\angle_{arene}$) can be calculated – 11.43(11)° for **2Sc**, and 12.9(3)° for **2La**. In **2Sc**, the next shortest $M\cdots C_{6\text{-centroid}}$ distance (3.8304(7) Å) is too long to constitute a strong interaction; but, in **2La** the equivalent group is only *ca*. 0.4 Å further ($M\cdots C_{6\text{-centroid}}$ = 2.8348(12) Å) than the deformed arene ring, but is planar. Complex **2Sc** is similar to the Ti(IV) analogue **2Ti**,[44] but the latter exhibits $\angle_{arene}$ of 24.19(18)° and is diamagnetic by SQUID magnetometry, indicating the presence of a dianionic Tripp ring.

Complex **2Y** is different to **2Sc** and **2La** as only half the molecule is present in the asymmetric unit (Z' = 0.5), as previously reported;[36] and also to that of **2U**.[45] The $\angle_{arene}$ angle for both ligands in **2Y** is 7.27(12)°, which compares well to 9.5(1)° in **2U.**[45] There is no clear trend in $\angle_{arene}$ values (**2Y** < **2U** < **2La** < **2Sc**) except that C_2 symmetric complexes (**2Y** and **2U**) have smaller $\angle_{arene}$ angles,[36, 45] and that larger values (with a single deformed arene) correlate with a greater degree of metal electron localisation (see below). The Gd(0) complex, $[Gd(C_6H_3\text{-}1,3,5\text{-}t\text{Bu})_2]$, also displays two symmetry-equivalent distorted arene rings ($\angle_{arene}$ = 3.1(3)°).[31] The remaining divalent complexes, **2Sm**, **2Eu**, **2Tm**, and **2Yb**, are analogous to **2La**, except only the latter shows arene deformation. **Table 1** summarizes all **2M** complexes now reported (M = Sc, Y, La, Sm, Eu, Tm, Yb, U).[36, 45]

Table 1. Bond lengths (Å) and angles (°) for [M(NHAr^{iPr6})$_2$] (**2M**, M = Sc, Y, La, Sm, Eu, Tm, Yb, U).[36, 45]

(Å or °)	2Sc	2Y [A]	2La	2Sm	2Eu [B]	2Tm	2Yb [B]	2U
M–N N(1)	2.0884(11)	2.2600(12)	2.395(3)	2.412(2)	2.411(4) 2.414(5) [B]	2.3060(17)	2.310(6) 2.294(6) [B]	2.330(2)
N(2)	2.0678(10)	– [A]	2.434(3)	2.425(2)	– [B]	2.3169(18)	– [B]	– [A]
M–C$_{6\text{-range}}$ Ring(1)	2.3913(12)– 2.6304(14)	2.7276(14)– 2.9273(15)	2.778(16)– 2.971(9)	2.955(3)– 3.160(3)	2.972(4)– 3.176(5)	2.8015(19)– 2.971(2)	2.840(6)– 3.047(6)	2.723(3)– 2.870(3)
Ring(2)	–	– [A]	3.047(3)– 3.240(3)	2.953(3)– 3.201(3)	– [B]	2.819(2)–3.118(2)	– [B]	– [A]
M–C C(8)	2.3913(12)	2.7684(14)	2.843(13)	–	–	–	–	2.731(3)
C(11)	2.5418(13)	2.7859(15)	2.903(12)	–	–	–	–	2.723(3)
Arene fold angle	11.43(11)	7.27(12)	12.9(9)	–	–	–	–	9.3(2)

[A] The solid-state structure is C_2-symmetric so there is a single metal and ligand per asymmetric unit; [B] The solid-state structures show two half-molecules in the asymmetric unit, so M(1) and M(2) each have only one unique ligand

UV-Vis-NIR spectroscopy

UV-Vis-NIR spectra were collected for **1M** (M = Sc, Y, La, Tm) and **2M** (M = Sc, Y, La, Sm, Eu, Yb) at ambient temperature as 1 mM solutions in Et_2O (**Figure 2**, except for **1Tm**). The spectra of **1Sc**, **1Y**, and **1La** are uninformative, showing only a broad ligand-to-metal charge transfer (LMCT) process from *ca*. 20,000 cm^{-1} (500 nm) to well into the UV region, accounting for the intense yellow colour of all three in solution. The colours and spectra of **1Tm** and **2Sm**, **2Eu**, **2Tm**, and **2Yb** are typical for these elements in their respective oxidation states (see *Supporting Information*).[13, 14, 46-49]

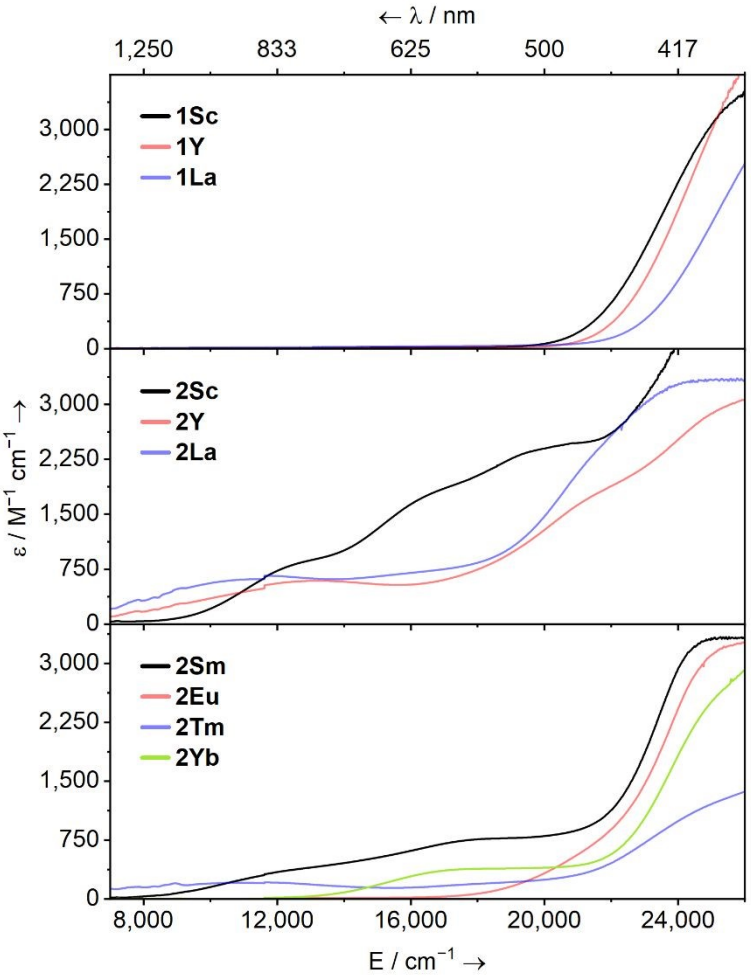

Figure 2. Solution UV-Vis-NIR spectra of [M(NHAr^{i}Pr6)(I)] (**1M**, M = Sc, Y, La; top) and [M(NHAr^{i}Pr6)] (**2M**, middle, M = Sc, Y, La; bottom, M = Sm, Eu, Tm, Yb) – as 1 mM solutions in Et_2O between 7,000–26,000 cm^{-1} (1,429–385 nm) at ambient temperature.

View Article Online
DOI: 10.1039/D4SC03005B

The spectrum of **2Sc** shows three well-resolved absorptions at 13,400 cm^{-1} (756 nm, 805 M^{-1} cm^{-1}), 17,400 cm^{-1} (575 nm, 1,727 M^{-1} cm^{-1}), and 21,300 cm^{-1} (469 nm, 2,471 M^{-1} cm^{-1}). The modest intensity of these peaks coupled with their energies suggests $3d \rightarrow 3d$ transitions and/or metal-to-ligand charge transfer (MLCT) bands. For **2Y**, two peaks are resolved at 13,700 cm^{-1} (729 nm, 594 M^{-1} cm^{-1}) and 21,600 (463 nm, 1,787 M^{-1} cm^{-1}), while a third tails in from above 26,000 cm^{-1} (385 nm), in agreement with the previous report.[36] Finally, in **2La**, a single clear peak is resolved at 12,300 cm^{-1} (816 nm, 650 M^{-1} cm^{-1}), which we suggest is a $5d \rightarrow 5d$ transition. A broad feature at *ca*. 16,000 cm^{-1} and a peak with a maximum at *ca*. 24,000 cm^{-1} (417 nm) can also be seen, but background absorption precludes accurately describing these.

SQUID magnetometry

Direct current (DC) magnetic susceptibility data were collected for **1Tm**, and **2M** (M = Sc, Y, La, Sm, Eu, Tm) from 1.8 to 300 K under an applied field of 1 kOe. At 300 K, the $\chi_M T$ (χ_M is the molar magnetic susceptibility) values for **1Tm** (6.61 cm^3 mol^{-1} K), **2Eu** (7.27 cm^3 mol^{-1} K), and **2Tm** (2.47 cm^3 mol^{-1} K) closely match theoretical values for $4f^{n+1}$ configurations for Tm(III), $4f^{12}$ ($^3H_6$, 7.15 cm^3 mol^{-1}), Eu(II), $4f^7$ ($^8S_{7/2}$, 7.88 cm^3 mol^{-1} K), and Tm(II), $4f^{13}$ ($^2F_{7/2}$, 2.57 cm^3 mol^{-1} K). For **2Sm** ($4f^6$) the value at 300 K is 1.43 cm^3 mol^{-1} K, which is in the range observed for Eu(III) ($4f^6$) complexes (1.3 to 1.5 cm^3 mol^{-1} K),[50] and is non-zero due to population of excited ^7F_J states.[46-48] Upon cooling to 1.8 K, $\chi_M T$ for **2Sm** lowers to 0.02 cm^3 mol^{-1} K which is consistent with a $^7F_0$ ground state; thus, a $4f^6$ configuration.

Complexes **2Sc**, **2Y** and **2La** exhibit $\chi_M T$ values at 300 K (0.31, 0.36, and 0.29 cm^3 mol^{-1} K respectively), which are in reasonable agreement with the spin-only value for an $S = {}^1/_2$

View Article Online
DOI: 10.1039/D4SC03005B

system (0.375 m^3 mol^{-1} K for g = 2.00), and hence with a formal d^1 configuration. In each case, the magnetic moment is essentially invariant with temperature down to 8–10 K, where a sudden drop can be seen, though this varies across independently synthesized samples (see *Supporting Information* for more details).

Electronic structure calculations

Unrestricted Kohn-Sham density-functional theory (DFT) calculations were performed on **2Sc**, **2Y**, **2La**, **2Tm** (S = $^1/_2$), **2Sm** (S = 3), **2Eu** (S = $^7/_2$), and **2Yb** (S = 0) using partially geometry-optimized structures (see *Supporting Information* for full details). Löwdin population and spin analyses of **2Sm**, **2Eu**, **2Yb**, and **2Tm** are consistent with experimental data and describe all four as $4f^{n+1}$ Ln(II) ions with metal-localised valence electrons. **Figure 3A** and **C** shows the SOMOs of **2Sc** and **2La**, which depict M–arene δ-bonds comprised of 36% 3*d* (with 4% 4*s*) and 14% 5*d* (with 10% 4*f* and 1% 6*s*) metal character, respectively, with the bound Tripp ring making up 41% (**2Sc**) and 56% (**2La**) – the remainder is diffused over the rest of the molecule. Defining the M···Tripp direction as z, the *d*-orbital contribution is described as $d_{(xy/x2-y2)}$ (the superficial resemblance to d_{x2} or d_{y2} is due to a small degree of d_{z2} mixing in this axis system) – this is comparable to the e_{2g} MO of *bis*-benzene transition metal complexes in D_{6h} symmetry.[51]

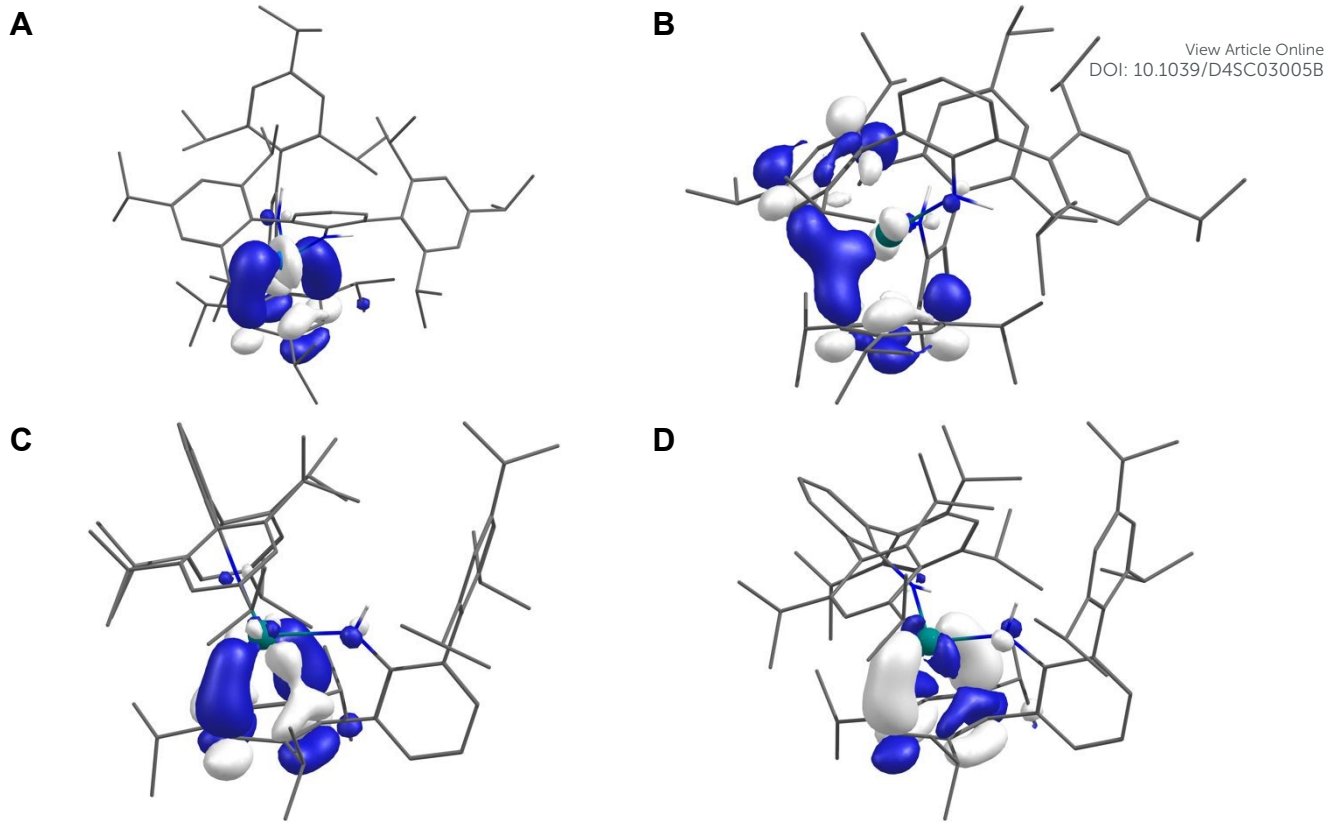

Figure 3. SOMOs of: (A) **2Sc**; (B) **2Y**; (C) **2La**; (D) **2Y-Et$_2$O** (isovalues = 0.05) using geometries derived from single crystal X-ray diffraction with H-atoms optimized (**2Sc**, **2Y**), select disordered C-atoms and all H-atoms optimized (**2La**), or all atom positions optimised (**2Y-Et$_2$O**). H-atoms except those of the N(H) group omitted for clarity.

In the case of **2Y** (**Figure 3B**), the SOMO is delocalized across the symmetry equivalent metal-bound Tripp groups such that the SOMO composition is 14% Y (12% 4*d*, 0.5% 5*s*), while the bound Tripp rings sum to 64.6% – the SOMO resembles a delocalized δ-bonding interaction. These results agree with previous work on **2Y**,[36] but it is an outlier compared to **2Sc** and **2La**. Full geometry optimisation of **2Y** using the lower-symmetry structure of **2La** as the starting point was performed in the gas phase and an Et_2O solvent model (**2Y-Et$_2$O** henceforth). Both calculations produced geometries that have only one metal-bound Tripp group deformed (*i.e.* like **2Sc** and **2La**) and are true local minima on the potential energy surface. **Figure 3D** shows the SOMO of **2Y-Et$_2$O**, and Löwdin population analysis shows it to be more metal-localized (22% 4*d*, 2% 5*s*, and 1% 4*f* – total 25%) than in the C_2-symmetric

View Article Online
DOI: 10.1039/D4SC03005B

2Y (14%), which is accompanied by a corresponding decrease in Tripp contributions to the SOMO – 65% in **2Y** (over two Tripp groups) and 56% in **2Y-Et$_2$O** (over a single Tripp group). The Löwdin spin populations at the metal in **2Y-Et$_2$O** (0.245) and **2Y** (0.142) reflect these differences.

Time-dependent DFT (TD-DFT) and simplified TD-DFT (sTD-DFT) calculations were employed to model the UV-Vis-NIR spectra of **2Sc**, **2Y**, **2La**, and **2Y-Et$_2$O**; here we focus on sTD-DFT with TPSSh for consistency with prior art (**Figure 4**),[11, 12, 16, 23, 52-54] see *Supporting Information* (**Figures S102** to **S111**) for more details. Experimental features of **2Sc** and **La** are well represented, and the Natural Transition Orbitals (NTOs) suggests the broad features in the spectrum of **2Sc** are 3*d*→3*d* transitions, the lowest energy of which resembles a $3d_{(xy/x2\text{-}y2)} \rightarrow 3d_{(x2\text{-}y2/xy)}$ transition maintaining the δ-bonding interaction. For **2La**, the lowest energy feature is a $5d_{(xy/x2\text{-}y2)} \rightarrow 5d_{(x2\text{-}y2/xy)}$ transition, and the next two lowest energy features are a combination of MLCT and $5d \rightarrow 5d$ transitions. There is poor agreement with all methods for **2Y** (**Figure 4** middle panel, red line), however, calculations for **2Y-Et$_2$O** are substantially better (**Figure 4** middle panel, blue line); this suggests that the structure of **2Y** in Et_2O solution is similar to the solid-state structures of **2Sc** and **2La**. The lowest energy feature in **2Y-Et$_2$O** is comprised of two components, a $4d_{(xy/x2\text{-}y2)} \rightarrow 4d_{(x2\text{-}y2/xy)}$ transition and an MLCT process.

View Article Online
DOI: 10.1039/D4SC03005B

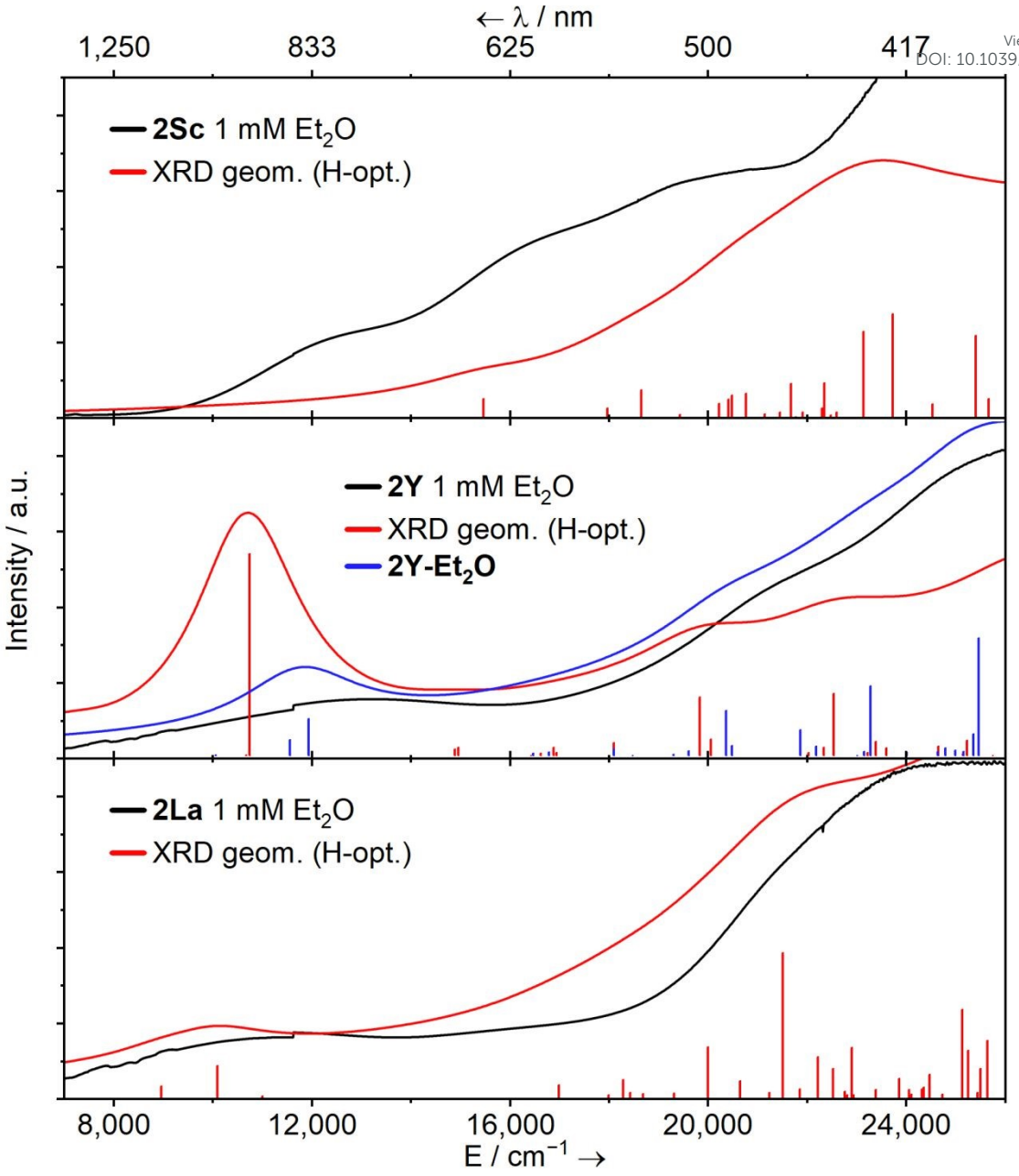

Figure 4. Experimental (1 mM, Et_2O, black), calculated sTD-DFT transitions (red and blue vertical lines), and simulated spectra (red and blue solid lines, with Gaussian broadening and a linewidth factor of $25 \times \sqrt{E}$) UV-Vis-NIR spectra for complexes **2Sc**, **2Y** (and **2Y-Et_2O**) and **2La** Calculated transitions were performed using a solvent model accounting for the dielectric constant (ε) and refractive index (n_D) of Et_2O.

Complete active space self-consistent field (CASSCF) calculations (see *Supporting Information*) on **2M** confirm the DFT and experimental results: **2Sc**, **2Y** and **2La** exhibit nd^1

View Article Online
DOI: 10.1039/D4SC03005B

ground states with significant orbital mixing with the arene ligand(s), and **2Sm**, **2Eu**, **2Tm** and **2Yb** have $4f^{n+1}$ ground states. Calculations for the lowest-lying excitations in **2Sc**, **2Y** and **2La** including multi-configurational pair-density functional theory (MC-PDFT) corrections for dynamic correlation show n*d*/arene→n*d*/arene excitations in the UV-Vis-NIR range, in good agreement with the experimental spectra. The character of these excitations is broadly in line with that found using (s)TD-DFT, where the lowest-lying excitations for **2Sc** are mostly localized to one side of the molecule and resemble *d*→*d* transitions, while some for **2La** and **2Y-Et$_2$O** are combined MLCT and 5*d*→5*d* transitions to the opposite Tripp ring.

EPR spectroscopy

Continuous wave (c.w.) EPR spectroscopy was used to study the orbitally non-degenerate species **2Sc**, **2Y** and **2La**. All three are EPR active as polycrystalline solids and in solution (1 mM Et_2O or *n*Pr_2O); spectra of **2Y** in Et_2O have been reported previously.[36] We find better resolved frozen solution spectra in *n*Pr_2O than in Et_2O (although the spectra are consistent; see *Supporting Information*).

X-band spectra of powders at room temperature show features around $g = 2$, consistent with the formal M(II) oxidation states. There is partial resolution of the metal hyperfine for **2Sc** (^{45}Sc, $I = 7/2$, 100% abundant) and **2Y** (^{89}Y, $I = 1/2$, 100%) but is unresolved for **2La** (^{139}La, $I = 7/2$, 100%). For **2Sc**, a hyperfine octet is observed, with $g = 2.000$ and $A = 145$ MHz, for **2Y** we observe a hyperfine doublet (estimated $A = 14$ MHz) with $g_\perp = 2.005$ and $g_\parallel = 1.995$, and for **2La**, we observe $g_\perp = 2.019$ and $g_\parallel = 1.958$. There are small changes in these parameters upon cooling to 5 K, without any improvement in resolution; the limited resolution of the powder spectra is indicative of intermolecular magnetic interactions.

View Article Online
DOI: 10.1039/D4SC03005B

Fluid solution spectra of **2Y** and **2La** (**Figure 5**, **Table 2**) give a hyperfine doublet (A_{iso} = 46 MHz, g_{iso} = 1.9995) and octet (A_{iso} = 112 MHz, g_{iso} = 1.998), respectively. For **2Sc** (**Figure 5**, **Table 2**) we also obtain an octet (A_{iso} = 205 MHz, g_{iso} = 1.989), but there is a second minor octet spectrum which differs subtly in the magnitude of the hyperfine (A_{iso} = 186 MHz), suggesting two Sc(II) species in solution with a relative abundance of *ca*. 12:1 (similar features have been observed recently in a different Sc(II) system[23]). In each case $g_{iso} < g_e$, consistent with the formal d^1 configuration. The isotropic part of the hyperfine interaction derives from *s*-orbital spin density, and from theoretical values of the hyperfine interaction for unit population of the valence *s*-orbitals[55] we estimate 7.3% (**2Sc**), 3.7% (**2Y**) and 2.0% (**2La**) *s*-orbital character of the SOMO; these are in good agreement with DFT calculations (3.6%, 1.8%, and 1.0% *s*-orbital character, or 3.8%, 2.0%, 1.1% Löwdin *s*-orbital spin populations). In summary, **2Sc** has the largest metal valence *s*-orbital spin density, then **2Y** > **2La**.

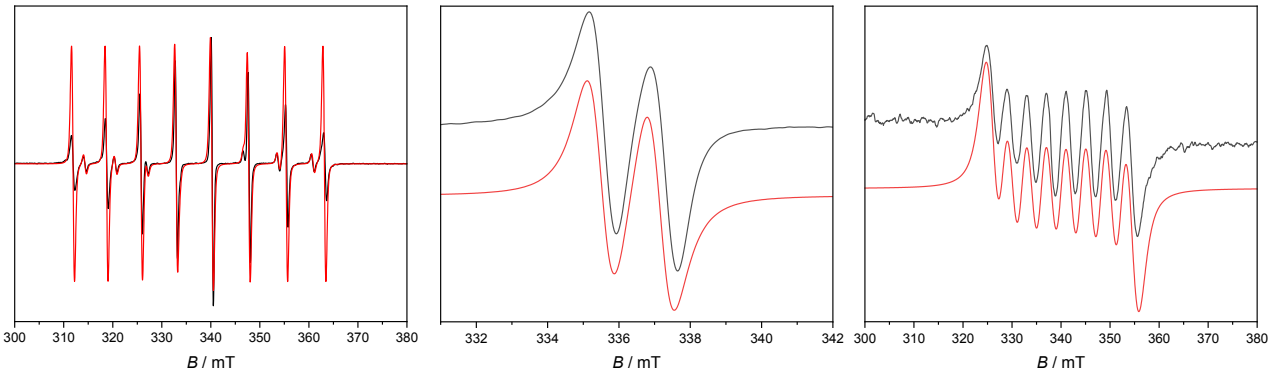

Figure 5. X-band c.w. EPR spectrum of 1 mM **2Sc** in Et_2O at 250 K (left), **2Y** in nPr_2O at 180 K (middle), and **2La** in Et_2O at 200 K (right). Black, experimental; red, simulations with parameters in the text.

View Article Online
DOI: 10.1039/D4SC03005B

Frozen solutions gave well-resolved spectra in each case (**Figure 6**, **Table 2**). For **2Sc** there is a dominant perpendicular hyperfine coupling $A_{\perp} \approx 210$ MHz ($g_{\perp} = 2.002$), from which we can determine $A_{\parallel} \approx 195$ MHz (using $A_{iso} = 205$ MHz from the fluid spectra), and by simulation we find $g_{\parallel} = 1.99$. However, these parameters are not well defined as there is evidence of a second species. For **2Y** and **2La** the spectra appear axially symmetric giving $g_{\perp} = 2.004$, $g_{\parallel} = 1.986$, with a near isotropic metal hyperfine of $A_{\perp} = 39$, $A_{\parallel} = 36$ MHz for **2Y**, while for **2La** we find $g_{\perp} = 2.005$, $g_{\parallel} = 1.952$ with $A_{\perp} = 110$, $A_{\parallel} = 100$ MHz.

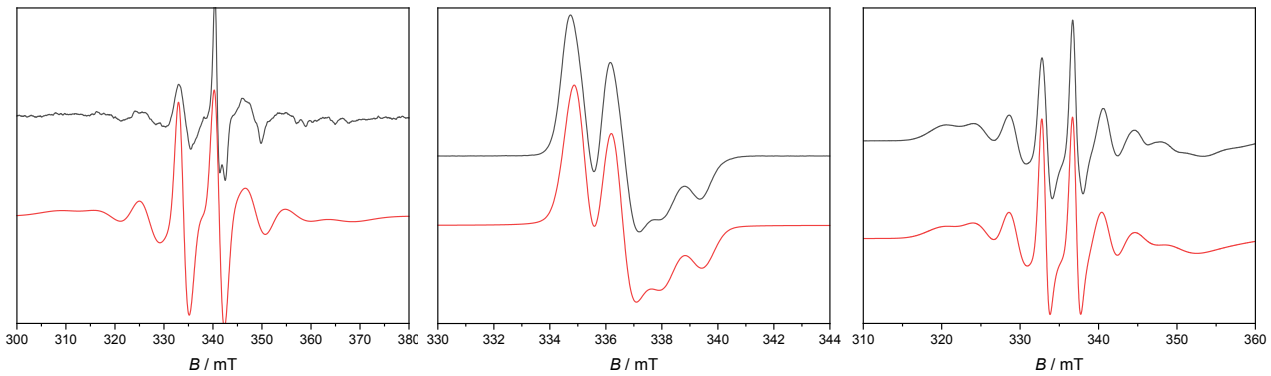

Figure 6. X-band c.w. EPR spectrum of 1 mM **2Sc** (left) in Et_2O at 130 K, **2Y** (middle) and **2La** (right) in nPr_2O at 60 K. Black experimental, red simulations.

Table 2. Experimental (frozen solution) and calculated EPR parameters for **2Sc**, **2Y** and **2La**. Calculated hyperfine coupling constants in MHz; experimental A_{iso} calculated as ($A_{\parallel}$ + $2A_{\perp}$)/3. The calculated g_1/A_1 axes are along the M-bound arene direction.

		g_1	g_2	g_3	A_1	A_2	A_3	A_{iso}
2Sc	Exp.	1.990	2.002		195	210		205
	Calc.	1.990	2.009	2.015	159	171	184	171
2Y	Exp.	1.986	2.004		36	39		38
2Y-Et_2O	Calc.	1.983	2.004	2.006	−47	−49	−50	−48
2La	Exp.	1.952	2.005		100	110		107
	Calc.	1.954	1.971	1.993	101	106	108	105

View Article Online
DOI: 10.1039/D4SC03005B

The anisotropy of the *g*-values for **2Sc**, **2Y** and **2La** is due to the significant *d*-orbital character of the SOMO. The $g_{\perp} > g_{\parallel}$ pattern indicates a dominant d_{x2-y2} contribution (where z is the M-bound arene direction), while the greater deviation of $g_{\parallel}$ from g_e in the series **2La** > **2Y** > **2Sc** is in keeping with greater spin-orbit coupling for the heavier elements,[56] and also the trend in the lowest energy excited states (see above). A simple analysis of the anisotropic metal hyperfine interaction to give the metal d_{x2-y2} contribution to the SOMO [$A_{\parallel} - A_{\perp} = (-6/7)a^2P_d$, where *a* is the d_{x2-y2} coefficient of the SOMO and P_d is tabulated[55]] gives 7.3% for **2Sc**, 5.6% for **2Y** and 4.9% for **2La**. DFT calculations give much larger *d*-orbital contributions of 36%, 20%, and 14%, respectively (see above), despite also showing reasonable agreement with the measured hyperfine coupling constants (**Table 2**), implying an inadequacy in the simple analysis above; we have previously noted similar discrepancies in related $[M^{II}L_3]^-$ systems (M = Sc, Y, La, Lu).[17]

Indeed, the EPR parameters and electronic structures of **2Sc**, **2Y** and **2La** contrast to those related d^1 $[M^{II}L_3]^-$ species where the trigonal crystal field instead stabilises the d_{z2} (defined by the C_3 axis) orbital, or a *d*/*s* hybrid giving rise to characteristic $g_{\perp} < g_{\parallel}$ ($\approx g_e$) patterns.[2, 16, 17] The electronic structures of the present compounds have more in common with $[Sc(Cp^{ttt})_2]$,[23] where DFT calculations give a d_{x2-y2}-dominated SOMO, and a similar $g_{\perp} > g_{\parallel}$ pattern can be observed from the frozen solution EPR data. The hyperfine coupling in **2Y** and **2La** is much weaker than in the trigonal M(II) cyclopentadienyl species: for example, $[Y(Cp^R)_3]^-$ with various substituents [*e.g.* $(Cp^R)_3$ = Cp'$_3$, Cp$^t_3$, {Cp''$_2$(C$_5$H$_5$)}] have $|A_{iso}|$ = 98–130 MHz;[17, 57, 58] and $[La(Cp^R)_3]^-$ (Cp^R = Cp', Cp'', Cp^{tt}) have $|A_{iso}|$ = 390–640 MHz.[2, 17, 59] Hence, there is greater metal character in the SOMOs of $[M(Cp^R)_3]^-$ than in **2M**. Comparing the present compounds with more symmetric sandwich compounds, $[Y(Cp^{iPr5})_2]$ and $[La(Cp^{iPr5})_2]$ have larger magnitude $|A_{iso}|$ = 505 and 2000 MHz, respectively,[14] while curiously

View Article Online
DOI: 10.1039/D4SC03005B

$[Sc(Cp^{ttt})_2]$ has smaller magnitude $|A_{iso}|$ = 83 MHz,[23] although it has been reported that $[Sc(Cp^*)_2]$ (not structurally authenticated) has $|A_{iso}|$ = 824 MHz.[23]

Conclusions

In summary, we have reported a series of room-temperature stable crystalline divalent rare earth *bis*-tethered arene complexes of the form $[M(NHAr^{iPr6})_2]$ (**2M**; M = Sc, Y, La, Sm, Eu, Tm, Yb). In the case of Sc and La, these represent the second examples of neutral divalent complexes with these elements and are amongst just a few in any charge state. All **2M** complexes feature close metal-arene contacts, which in **2Sc**, **2Y**, and **2La**, results in an "open book" arene deformation suggestive of charge transfer, whereas in **2Sm**, **2Eu**, **2Tm**, and **2Yb** the equivalent arene groups remain planar. SQUID magnetometry and UV-Vis-NIR spectroscopy demonstrate **2Sm**, **2Eu**, **2Tm**, and **2Yb** are examples of $4f^{n+1}$ ions, and quantum chemical calculations show that the metal-localised 4*f* orbitals do not interact with the arene π-orbitals.

Solution-phase c.w. EPR spectroscopy of **2Sc**, **2Y**, and **2La** are consistent with formal nd^1 ions, where the SOMO has $nd_{(x2-y2)}$ character with delocalisation of the spin onto the Tripp groups. Quantum chemical and *ab initio* calculations further support this description and reveal mixing between metal $nd_{(x2-y2)}$ and arene-π orbitals to give δ-bonds, which explain the arene deformation in their structures.

The electronic structures of nd^1 **2Sc**, **2Y**, and **2La** closely resemble those of *bis*-benzene transition metal complexes; and, going forward, we posit that these rare $nd_{(x2-y2)}$ configurations afford as-yet unexplored opportunities to tune the physicochemical properties of divalent rare earth ions with formal $\{5d/6s\}^1$ valence electron configurations. This, along

with work to probe the limits of the *bis*-{NHAr$^{i\text{Pr}6}$} framework to stabilise other divalent *f*-block ions, remains an active area of research in our laboratory.

View Article Online
DOI: 10.1039/D4SC03005B

Conflicts of Interest

There are no conflicts to declare.

Acknowledgements

We thank the Royal Society for a University Research Fellowship (URF\211271 to C.A.P.G, and URF\191320 to N.F.C.); and the UoM Department of Chemistry for the funding of a PhD studentship under EPSRC DTP (EP/W524347/1 to R.E.M, and EP/T517823/1 to T.H). We acknowledge funding from the EPSRC (EP/K039547/1, EP/V007580/1, and EP/P001386/1 for NMR spectroscopy and X-ray diffraction). We also thank the EPSRC UK EPR National Research Facility including for access to the SQUID magnetometer (EP/W014521/1, EP/V035231/1, EPS033181/1). C.A.P.G and N.F.C. also thank the Computational Shared Facility at the University of Manchester for support. We thank Prof. Stephen Liddle for support (J.A.S). Elemental analyses were performed at the UoM by Mr Martin Jennings and Ms Anne Davies. We are also grateful to Profs. Aaron Odom and Selvan Demir for scientific discussions and encouragement.

Supporting Information

See the *Supporting Information* for details of the starting materials used, descriptions of sample preparation for spectroscopic measurements, and methodologies and coordinates

View Article Online
DOI: 10.1039/D4SC03005B

for the DFT and CASSCF calculations. The following CCDC references contain the supplementary crystal data for this article: **1Sc** (2266263), **1Y** (2266261), **1La** (2266235), **1Tm** (2266255), **1Yb** (2266257), **1Y$^{\beta}$** (2295306), **1La$^{\beta}$** (2295307), **2Sc** (2266264), **2Y** (2266262), **2La** (2266236), **2Sm** (2266243), **2Eu** (2266244), **2Tm** (2266256), **2Yb** (2266258), and **3** (2282041). These data can be obtained free of charge from the Cambridge Crystallographic Data Centre via *www.ccdc.cam.ac.uk/data_request/cif*. Raw experimental data (NMR, ATR-IR, UV-Vis-NIR, SQUID Magnetometry) and computational inputs/outputs can be found freely at DOI: 10.48420/25245760. The authors have cited additional references within the Supporting Information.[60-113]

References

1. K. R. Meihaus, M. E. Fieser, J. F. Corbey, W. J. Evans and J. R. Long, *J. Am. Chem. Soc.*, 2015, **137**, 9855-9860.
2. J. Liu, L. E. Nodaraki, D. O. T. A. Martins, M. J. Giansiracusa, P. J. Cobb, J. Emerson-King, F. Ortu, G. F. S. Whitehead, G. K. Gransbury, E. J. L. Mclnnes, F. Tuna and D. P. Mills, *Eur. J. Inorg. Chem.*, 2023, **26**, e202300552.
3. M. R. MacDonald, J. W. Ziller and W. J. Evans, *J. Am. Chem. Soc.*, 2011, **133**, 15914-15917.
4. M. R. MacDonald, J. E. Bates, M. E. Fieser, J. W. Ziller, F. Furche and W. J. Evans, *J. Am. Chem. Soc.*, 2012, **134**, 8420-8423.
5. M. R. MacDonald, J. E. Bates, J. W. Ziller, F. Furche and W. J. Evans, *J. Am. Chem. Soc.*, 2013, **135**, 9857-9868.
6. M. E. Fieser, M. G. Ferrier, J. Su, E. Batista, S. K. Cary, J. W. Engle, W. J. Evans, J. S. Lezama Pacheco, S. A. Kozimor, A. C. Olson, A. J. Ryan, B. W. Stein, G. L. Wagner, D. H. Woen, T. Vitova and P. Yang, *Chem. Sci.*, 2017, **8**, 6076-6091.

View Article Online
DOI: 10.1039/D4SC03005B

7. M. T. Trinh, J. C. Wedal and W. J. Evans, *Dalton Trans.*, 2021, **50**, 14384-14389.
8. T. F. Jenkins, D. H. Woen, L. N. Mohanam, J. W. Ziller, F. Furche and W. J. Evans, *Organometallics*, 2018, **37**, 3863-3873.
9. A. J. Ryan, L. E. Darago, S. G. Balasubramani, G. P. Chen, J. W. Ziller, F. Furche, J. R. Long and W. J. Evans, *Chem. Eur. J.*, 2018, **24**, 7702-7709.
10. S. A. Moehring, M. Miehlich, C. J. Hoerger, K. Meyer, J. W. Ziller and W. J. Evans, *Inorg. Chem.*, 2020, **59**, 3207-3214.
11. D. N. Huh, S. R. Ciccone, S. Bekoe, S. Roy, J. W. Ziller, F. Furche and W. J. Evans, *Angew. Chem., Int. Ed.*, 2020, **59**, 16141-16146.
12. L. M. Anderson-Sanchez, J. M. Yu, J. W. Ziller, F. Furche and W. J. Evans, *Inorg. Chem.*, 2023, **62**, 706-714.
13. M. E. Fieser, M. R. MacDonald, B. T. Krull, J. E. Bates, J. W. Ziller, F. Furche and W. J. Evans, *J. Am. Chem. Soc.*, 2015, **137**, 369-382.
14. K. R. McClain, C. A. Gould, D. A. Marchiori, H. Kwon, T. T. Nguyen, K. E. Rosenkoetter, D. Kuzmina, F. Tuna, R. D. Britt, J. R. Long and B. G. Harvey, *J. Am. Chem. Soc.*, 2022, **144**, 22193-22201.
15. P. W. Smith, J. Hrubý, W. J. Evans, S. Hill and S. G. Minasian, *J. Am. Chem. Soc.*, 2024, **146**, 5781-5785.
16. K. Kundu, J. R. K. White, S. A. Moehring, J. M. Yu, J. W. Ziller, F. Furche, W. J. Evans and S. Hill, *Nat. Chem.*, 2022, **14**, 392-397.
17. A.-M. Ariciu, D. H. Woen, D. N. Huh, L. E. Nodaraki, A. K. Kostopoulos, C. A. P. Goodwin, N. F. Chilton, E. J. L. McInnes, R. E. P. Winpenny, W. J. Evans and F. Tuna, *Nat. Commun.*, 2019, **10**, 3330.
18. C. A. Gould, K. R. McClain, J. M. Yu, T. J. Groshens, F. Furche, B. G. Harvey and J. R. Long, *J. Am. Chem. Soc.*, 2019, **141**, 12967-12973.

View Article Online
DOI: 10.1039/D4SC03005B

19. P.-B. Jin, Q.-C. Luo, G. K. Gransbury, I. J. Vitorica-Yrezabal, T. Hajdu, I. Strashnov, E. J. L. McInnes, R. E. P. Winpenny, N. F. Chilton, D. P. Mills and Y.-Z. Zheng, *J. Am. Chem. Soc.*, 2023, **145**, 27993-28009.

20. C. A. Gould, K. R. McClain, D. Reta, J. G. C. Kragskow, D. A. Marchiori, E. Lachman, E. S. Choi, J. G. Analytis, R. D. Britt, N. F. Chilton, B. G. Harvey and J. R. Long, *Science*, 2022, **375**, 198-202.

21. J. C. Wedal, L. M. Anderson-Sanchez, M. T. Dumas, C. A. Gould, M. J. Beltran-Leiva, C. Celis-Barros, D. Paez-Hernandez, J. W. Ziller, J. R. Long and W. J. Evans, *J. Am. Chem. Soc.*, 2023, **145**, 10730-10742.

22. K. R. McClain, H. Kwon, K. Chakarawet, R. Nabi, J. G. C. Kragskow, N. F. Chilton, R. D. Britt, J. R. Long and B. G. Harvey, *J. Am. Chem. Soc.*, 2023, **145**, 8996-9002.

23. J. D. Queen, L. M. Anderson-Sanchez, C. R. Stennett, A. Rajabi, J. W. Ziller, F. Furche and W. J. Evans, *J. Am. Chem. Soc.*, 2024, **146**, 3279-3292.

24. J. T. Boronski, J. A. Seed, D. Hunger, A. W. Woodward, J. van Slageren, A. J. Wooles, L. S. Natrajan, N. Kaltsoyannis and S. T. Liddle, *Nature*, 2021, **598**, 72-75.

25. M. D. Straub, E. T. Ouellette, M. A. Boreen, R. D. Britt, K. Chakarawet, I. Douair, C. A. Gould, L. Maron, I. Del Rosal, D. Villarreal, S. G. Minasian and J. Arnold, *J. Am. Chem. Soc.*, 2021, **143**, 19748-19760.

26. J. D. Cryer and S. T. Liddle, in *Comprehensive Organometallic Chemistry IV*, eds. G. Parkin, K. Meyer and D. O'Hare, Elsevier, Oxford, 2022, pp. 460-501.

27. J. Murillo, R. Bhowmick, K. L. M. Harriman, A. Gomez-Torres, J. Wright, R. W. Meulenberg, P. Miro, A. Metta-Magana, M. Murugesu, B. Vlaisavljevich and S. Fortier, *Chem. Sci.*, 2021, **12**, 13360-13372.

28. R. A. Keerthi Shivaraam, M. Keener, D. K. Modder, T. Rajeshkumar, I. Zivkovic, R. Scopelliti, L. Maron and M. Mazzanti, *Angew. Chem., Int. Ed.*, 2023, **62**, e202304051.

View Article Online
DOI: 10.1039/D4SC03005B

29. M. Keener, R. A. K. Shivaraam, T. Rajeshkumar, M. Tricoire, R. Scopelliti, I. Zivkovic, A. S. Chauvin, L. Maron and M. Mazzanti, *J. Am. Chem. Soc.*, 2023, **145**, 16271-16283.

30. H. S. La Pierre, A. Scheurer, F. W. Heinemann, W. Hieringer and K. Meyer, *Angew. Chem., Int. Ed.*, 2014, **53**, 7158-71562.

31. J. G. Brennan, F. G. N. Cloke, A. A. Sameh and A. Zalkin, *J. Chem. Soc., Chem. Commun.*, 1987, 1668-1669.

32. D. M. Anderson, F. G. N. Cloke, P. A. Cox, N. Edelstein, J. C. Green, T. Pang, A. A. Sameh and G. Shalimoff, *J. Chem. Soc., Chem. Commun.*, 1989, 53-55.

33. W. A. King, T. J. Marks, D. M. Anderson, D. J. Duncalf and F. G. N. Cloke, *J. Am. Chem. Soc.*, 1992, **114**, 9221-9223.

34. F. G. N. Cloke, *Chem. Soc. Rev.*, 1993, **22**, 17-24.

35. W. A. King, S. Di Bella, G. Lanza, K. Khan, D. J. Duncalf, F. G. N. Cloke, I. L. Fragala and T. J. Marks, *J. Am. Chem. Soc.*, 1996, **118**, 627-635.

36. R. Jena, F. Benner, F. Delano, D. Holmes, J. McCracken, S. Demir and A. L. Odom, *Chem. Sci.*, 2023, **14**, 4257-4264.

37. P. Dorenbos, *J. Condens. Matter Phys.*, 2003, **15**, 575-594.

38. P. Dorenbos, *J. Lumin.*, 2000, **91**, 91-106.

39. B. R. Barnett, C. C. Mokhtarzadeh, P. Lummis, S. Wang, J. D. Queen, J. Gavenonis, N. Schüwer, T. D. Tilley, J. N. Boynton, N. Weidemann, D. W. Agnew, P. W. Smith, T. B. Ditri, A. E. Carpenter, J. K. Pratt, N. D. Mendelson, J. S. Figueroa and P. P. Power, in *Inorganic Syntheses*, 2018, pp. 85-122.

40. B. Twamley, C.-S. Hwang, N. J. Hardman and P. P. Power, *J. Organomet. Chem.*, 2000, **609**, 152-160.

41. K. Izod, S. T. Liddle and W. Clegg, *Inorg. Chem.*, 2004, **43**, 214-218.

42. P. Girard, J. L. Namy and H. B. Kagan, *J. Am. Chem. Soc.*, 1980, **102**, 2693-2698.

43. S. R. Chowdhury, C. A. P. Goodwin and B. Vlaisavljevich, *Chem. Sci.*, 2024, **15**, 1810-1819.
View Article Online
DOI: 10.1039/D4SC03005B

44. J. N. Boynton, J. D. Guo, F. Grandjean, J. C. Fettinger, S. Nagase, G. J. Long and P. P. Power, *Inorg. Chem.*, 2013, **52**, 14216-14223.

45. B. S. Billow, B. N. Livesay, C. C. Mokhtarzadeh, J. McCracken, M. P. Shores, J. M. Boncella and A. L. Odom, *J. Am. Chem. Soc.*, 2018, **140**, 17369-17373.

46. N. F. Chilton, C. A. P. Goodwin, D. P. Mills and R. E. P. Winpenny, *Chem. Commun.*, 2015, **51**, 101-103.

47. C. A. P. Goodwin, K. C. Joslin, S. J. Lockyer, A. Formanuik, G. A. Morris, F. Ortu, I. J. Vitorica-Yrezabal and D. P. Mills, *Organometallics*, 2015, **34**, 2314-2325.

48. C. A. P. Goodwin, N. F. Chilton, G. F. Vettese, E. Moreno Pineda, I. F. Crowe, J. W. Ziller, R. E. P. Winpenny, W. J. Evans and D. P. Mills, *Inorg. Chem.*, 2016, **55**, 10057-10067.

49. C. A. P. Goodwin, N. F. Chilton, L. S. Natrajan, M.-E. Boulon, J. W. Ziller, W. J. Evans and D. P. Mills, *Inorg. Chem.*, 2017, **56**, 5959-5970.

50. Y. Takikawa, S. Ebisu and S. Nagata, *J. Phys. Chem. Sol.*, 2010, **71**, 1592-1598.

51. V. M. Rayón and G. Frenking, *Organometallics*, 2003, **22**, 3304-3308.

52. A. Rajabi, R. Grotjahn, D. Rappoport and F. Furche, *Dalton Trans.*, 2024, **53**, 410-417.

53. M. E. Fieser, C. T. Palumbo, H. S. La Pierre, D. P. Halter, V. K. Voora, J. W. Ziller, F. Furche, K. Meyer and W. J. Evans, *Chem. Sci.*, 2017, **8**, 7424-7433.

54. C. T. Palumbo, D. P. Halter, V. K. Voora, G. P. Chen, A. K. Chan, M. E. Fieser, J. W. Ziller, W. Hieringer, F. Furche, K. Meyer and W. J. Evans, *Inorg. Chem.*, 2018, **57**, 2823-2833.

55. J. R. Morton and K. F. Preston, *J. Magn. Reson.*, 1978, **30**, 577-582.

View Article Online
DOI: 10.1039/D4SC03005B

56. S. Koseki, N. Matsunaga, T. Asada, M. W. Schmidt and M. S. Gordon, *J. Phys. Chem. A*, 2019, **123**, 2325-2339.

57. J. F. Corbey, D. H. Woen, C. T. Palumbo, M. E. Fieser, J. W. Ziller, F. Furche and W. J. Evans, *Organometallics*, 2015, **34**, 3909-3921.

58. M. A. Angadol, D. H. Woen, C. J. Windorff, J. W. Ziller and W. J. Evans, *Organometallics*, 2019, **38**, 1151-1158.

59. S. A. Moehring and W. J. Evans, *Organometallics*, 2020, **39**, 1187-1194.

60. W. T. Carnall and P. R. Fields, in *Lanthanide/Actinide Chemistry*, American Chemical Society, 1967, vol. 71, ch. 7, pp. 86-101.

61. M. Dolg, H. Stoll and H. Preuss, *J. Chem. Phys.*, 1989, **90**, 1730-1734.

62. M. Dolg, H. Stoll, A. Savin and H. Preuss, *Theoret. Chim. Acta*, 1989, **75**, 173-194.

63. D. Andrae, U. Häußermann, M. Dolg, H. Stoll and H. Preuß, *Theoret. Chim. Acta*, 1990, **77**, 123-141.

64. O. Kahn, *Molecular Magnetism*, VCH Publishers, Inc., New York, 1993.

65. J. P. Perdew, K. Burke and M. Ernzerhof, *Phys. Rev. Lett.*, 1996, **77**, 3865-3868.

66. J. P. Perdew, M. Ernzerhof and K. Burke, *J. Chem. Phys.*, 1996, **105**, 9982-9985.

67. V. Barone and M. Cossi, *J. Phys. Chem. A*, 1998, **102**, 1995-2001.

68. C. Adamo and V. Barone, *J. Chem. Phys.*, 1999, **110**, 6158-6170.

69. M. Ernzerhof and G. E. Scuseria, *J. Chem. Phys.*, 1999, **110**, 5029-5036.

70. N. Muller, P. C. Lauterbur and J. Goldenson, *J. Am. Chem. Soc.*, 2002, **78**, 3557-3561.

71. J. Tao, J. P. Perdew, V. N. Staroverov and G. E. Scuseria, *Phys. Rev. Lett.*, 2003, **91**, 146401.

72. Persistence of Vision Raytracer (Version 3.6); Persistence of Vision Pty. Ltd.: 2004. https://www.povray.org.

View Article Online
DOI: 10.1039/D4SC03005B

73. B. O. Roos, R. Lindh, P.-Å. Malmqvist, V. Veryazov and P.-O. Widmark, *J. Phys. Chem. A*, 2004, **108**, 2851-2858.

74. B. O. Roos, V. Veryazov and P.-O. Widmark, *Theor. Chem. Acc.*, 2004, **111**, 345-351.

75. V. N. Staroverov, G. E. Scuseria, J. Tao and J. P. Perdew, *J. Chem. Phys.*, 2004, **121**.

76. T. Yanai, D. P. Tew and N. C. Handy, *Chem. Phys. Lett.*, 2004, **393**, 51-57.

77. S. Grimme, *J. Phys. Chem. A*, 2005, **109**, 3067-3077.

78. B. O. Roos, R. Lindh, P.-Å. Malmqvist, V. Veryazov and P.-O. Widmark, *J. Phys. Chem. A*, 2005, **109**, 6575-6579.

79. B. O. Roos, R. Lindh, P.-Å. Malmqvist, V. Veryazov and P.-O. Widmark, *Chem. Phys. Lett.*, 2005, **409**, 295-299.

80. F. Weigend and R. Ahlrichs, *Phys. Chem. Chem. Phys.*, 2005, **7**, 3297-3305.

81. S. Grimme, *J. Comput. Chem.*, 2006, **27**, 1787-1799.

82. M. Reiher, *Theor. Chem. Acc.*, 2006, **116**, 241-252.

83. F. Weigend, *Phys. Chem. Chem. Phys.*, 2006, **8**, 1057-1065.

84. D. A. Pantazis, X. Y. Chen, C. R. Landis and F. Neese, *J. Chem. Theory. Comput.*, 2008, **4**, 908-919.

85. G. M. Sheldrick, *Acta Crystallogr. A*, 2008, **64**, 112-122.

86. W. Clegg, A. J. Blake, J. M. Cole, J. S. O. Evans, P. Main, S. Parsons and D. J. Watkin, *Crystal Structure Analysis*, Oxford University Press, Oxford, 2nd edn., 2009.

87. O. V. Dolomanov, L. J. Bourhis, R. J. Gildea, J. A. K. Howard and H. Puschmann, *J. Appl. Crystallogr.*, 2009, **42**, 339-341.

88. F. Neese, F. Wennmohs, A. Hansen and U. Becker, *Chem. Phys.*, 2009, **356**, 98-109.

89. D. A. Pantazis and F. Neese, *J. Chem. Theory. Comput.*, 2009, **5**, 2229-2238.

View Article Online
DOI: 10.1039/D4SC03005B

90. S. Grimme, J. Antony, S. Ehrlich and H. Krieg, *J. Chem. Phys.*, 2010, **132**, 154104.

91. S. Grimme, S. Ehrlich and L. Goerigk, *J. Comput. Chem.*, 2011, **32**, 1456-1465.

92. R. Izsak and F. Neese, *J. Chem. Phys.*, 2011, **135**, 144105.

93. D. A. Pantazis and F. Neese, *J. Chem. Theory. Comput.*, 2011, **7**, 677-684.

94. T. Noro, M. Sekiya and T. Koga, *Theor. Chem. Acc.*, 2012, **131**, 1124.

95. S. Grimme, *J. Chem. Phys.*, 2013, **138**, 244104.

96. C. Bannwarth and S. Grimme, *Comp. Theo. Chem.*, 2014, **1040-1041**, 45-53.

97. G. Li Manni, R. K. Carlson, S. Luo, D. Ma, J. Olsen, D. G. Truhlar and L. Gagliardi, *J. Chem. Theory. Comput.*, 2014, **10**, 3669-3680.

98. S. T. Liddle, *Angew. Chem., Int. Ed.*, 2015, **54**, 8604-8641.

99. S. T. Liddle and J. Van Slageren, *Chem. Soc. Rev.*, 2015, **44**, 6655-6669.

100. G. M. Sheldrick, *Acta Crystallogr. C*, 2015, **71**, 3-8.

101. D. Aravena, F. Neese and D. A. Pantazis, *J. Chem. Theory. Comput.*, 2016, **12**, 1148-1156.

102. G. Li Manni, R. K. Carlson, S. Luo, D. Ma, J. Olsen, D. G. Truhlar and L. Gagliardi, *J. Chem. Theory. Comput.*, 2016, **12**, 458-458.

103. I. L. Fedushkin, D. S. Yambulatov, A. A. Skatova, E. V. Baranov, S. Demeshko, A. S. Bogomyakov, V. I. Ovcharenko and E. M. Zueva, *Inorg. Chem.*, 2017, **56**, 9825-9833.

104. H. M. Nicholas, M. Vonci, C. A. P. Goodwin, S. W. Loo, S. R. Murphy, D. Cassim, R. E. P. Winpenny, E. J. L. McInnes, N. F. Chilton and D. P. Mills, *Chem. Sci.*, 2019, **10**, 10493-10502.

105. M. Xémard, M. Cordier, F. Molton, C. Duboc, B. Le Guennic, O. Maury, O. Cador and G. Nocton, *Inorg. Chem.*, 2019, **58**, 2872-2880.

106. D. Parker, E. A. Suturina, I. Kuprov and N. F. Chilton, *Acc. Chem. Res.*, 2020, **53**, 1520-1534.

107. J. D. Rolfes, F. Neese and D. A. Pantazis, *J. Comput. Chem.*, 2020, **41**, 1842-1849.

View Article Online
DOI: 10.1039/D4SC03005B

108. J. Liu, M. M. Bollmeyer, Y. Kim, D. Xiao, S. N. MacMillan, Q. Chen, X. Leng, S. H. Kim, L. Zhao, K. M. Lancaster and L. Deng, *J. Am. Chem. Soc.*, 2021, **143**, 10751-10759.

109. J. A. Seed, L. Birnoschi, E. Lu, F. Tuna, A. J. Wooles, N. F. Chilton and S. T. Liddle, *Chem*, 2021, **7**, 1666-1680.

110. F. Neese, *WIRES Comput. Mol. Sci.*, 2022, **12**, e1606.

111. Rigaku Oxford Diffraction, (2023), CrysAlisPro Software system, version 1.171.43, Rigaku Corporation, Wroclaw, Poland.; Rigaku Oxford Diffraction: 2023.

112. G. Li Manni, I. Fdez. Galván, A. Alavi, F. Aleotti, F. Aquilante, J. Autschbach, D. Avagliano, A. Baiardi, J. J. Bao, S. Battaglia, L. Birnoschi, A. Blanco-González, S. I. Bokarev, R. Broer, R. Cacciari, P. B. Calio, R. K. Carlson, R. Carvalho Couto, L. Cerdán, L. F. Chibotaru, N. F. Chilton, J. R. Church, I. Conti, S. Coriani, J. Cuéllar-Zuquin, R. E. Daoud, N. Dattani, P. Decleva, C. de Graaf, M. G. Delcey, L. De Vico, W. Dobrautz, S. S. Dong, R. Feng, N. Ferré, M. Filatov, L. Gagliardi, M. Garavelli, L. González, Y. Guan, M. Guo, M. R. Hennefarth, M. R. Hermes, C. E. Hoyer, M. Huix-Rotllant, V. K. Jaiswal, A. Kaiser, D. S. Kaliakin, M. Khamesian, D. S. King, V. Kochetov, M. Krośnicki, A. A. Kumaar, E. D. Larsson, S. Lehtola, M.-B. Lepetit, H. Lischka, P. López Ríos, M. Lundberg, D. Ma, S. Mai, P. Marquetand, I. C. D. Merritt, F. Montorsi, M. Mörchen, A. Nenov, V. H. A. Nguyen, Y. Nishimoto, M. S. Oakley, M. Olivucci, M. Oppel, D. Padula, R. Pandharkar, Q. M. Phung, F. Plasser, G. Raggi, E. Rebolini, M. Reiher, I. Rivalta, D. Roca-Sanjuán, T. Romig, A. A. Safari, A. Sánchez-Mansilla, A. M. Sand, I. Schapiro, T. R. Scott, J. Segarra-Martí, F. Segatta, D.-C. Sergentu, P. Sharma, R. Shepard, Y. Shu, J. K. Staab, T. P. Straatsma, L. K. Sørensen, B. N. C. Tenorio, D. G. Truhlar, L. Ungur, M. Vacher, V. Veryazov, T. A. Voß, O. Weser, D. Wu, X. Yang, D. Yarkony, C. Zhou, J. P. Zobel and R. Lindh, *J. Chem. Theory. Comput.*, 2023, **19**, 6933-6991.

113. GNU Image Manipulation Program (GIMP) (Version 2.10.38); The GIMP Team: 2024. https://www.gimp.org.

View Article Online
DOI: 10.1039/D4SC03005B

The following is already present under the “Supporting Information” heading:

View Article Online
DOI: 10.1039/D4SC03005B

The following CCDC references contain the supplementary crystal data for this article: **1Sc** (2266263), **1Y** (2266261), **1La** (2266235), **1Tm** (2266255), **1Yb** (2266257), **1Y$^{\beta}$** (2295306), **1La$^{\beta}$** (2295307), **2Sc** (2266264), **2Y** (2266262), **2La** (2266236), **2Sm** (2266243), **2Eu** (2266244), **2Tm** (2266256), **2Yb** (2266258), and **3** (2282041). These data can be obtained free of charge from the Cambridge Crystallographic Data Centre via *www.ccdc.cam.ac.uk/data_request/cif*. Raw experimental data (NMR, ATR-IR, UV-Vis-NIR, SQUID Magnetometry) and computational inputs/outputs can be found freely at DOI: 10.48420/25245760.